PHYSICAL REVIEW B VOLUME 21, NUMBER 1 1 JANUARY 1980

Electrical resistivity of the singlet-ground-state system $Tb_cY_{1-c}Sb$

N. Hessel Andersen, J. Jensen, H. Smith, and O. Splittorff
Physics Laboratory I, H. C. Ørsted Institute, University of Copenhagen, Denmark

O. Vogt
Laboratorium für Festkörperphysik, ETH, Zurich, Switzerland

(Received 7 February 1979)

The electrical resistivity of $Tb_cY_{1-c}Sb$ has been investigated as a function of temperature and Tb concentration in order to study the competing effects of the crystal field and the two-ion exchange interaction on the scattering of conduction electrons. The methods of growing and analyzing the crystals are outlined and the experimental technique of measuring the electrical resistivity is accounted for. A theoretical description of the scattering of conduction electrons from magnetic excitations is developed within a spherical model for the electronic energy bands. The resistivity is calculated using the random-phase approximation for the excitations of the $Tb_cY_{1-c}Sb$ system, both in the paramagnetic and the antiferromagnetically ordered phase. Satisfactory agreement with the experimental results is obtained for the entire range of concentration c by use of only one value for each of the two adjustable parameters, the Fermi momentum and the electron-ion exchange constant.

I. INTRODUCTION

The scattering of conduction electrons against the elementary excitations of a metal gives rise to a temperature-dependent resistivity, whenever the temperature is comparable to or less than a typical energy transfer involved in the collision. A well-known example is the scattering of electrons against the phonons of an ordinary metal. Another is the scattering of electrons against the magnetic excitations in metallic ferromagnets. A third example is the scattering of conduction electrons against individual magnetic-rare-earth ions which have their ground state split in energy by the crystal field of the lattice.

If the spectrum of elementary excitations has an energy gap Δ, one expects the temperature-dependent resistivity to be dominated at low temperatures by an exponential $e^{-\Delta/k_BT}$. When the electrons scatter against collective excitations without a gap, such as phonons or magnons in an isotropic ferromagnet, the low-temperature resistivity may be expected to show a power-law behavior, the details of which depend on the dispersion of the collective excitation and the form of the coupling constant for the interaction between the electron and the collective excitation.

Electrical-resistivity measurements on magnetic alloys may thus give information about the spectrum of elementary excitations and their coupling to the conduction electrons. By examining magnetic alloys like the $Tb_cY_{1-c}Sb$ system for $0 < c < 1$ one may also study the influence of spatial disorder on the magnetic excitations through their effect on the electrical resistivity. The disadvantage of this method when compared to, for instance, neutron scattering is the rather indirect nature of the information regarding the elementary excitations. Whereas a neutron scattering experiment picks out a particular wave number and frequency for the excitations, the electrical resistivity involves an integral over wave numbers and frequencies. In general one would therefore use the neutron scattering information on the collective excitations for the study of transport properties like electrical resistivity to obtain additional insight on the nature of the coupling between the conduction electrons and the elementary excitations. Sometimes, however, one can only get single crystals of rare-earth alloys in small size, which makes the use of inelastic neutron scattering difficult. In such cases the electrical-resistivity measurements may also provide valuable information on the nature of the magnetic excitations of the system.

A major experimental problem in measuring transport properties of rare-earth metals and alloys is their high content of impurities, which makes it difficult to measure the separate resistivity contribution due to inelastic scattering of the conduction electrons from the magnetic excitations. In the present study the samples used have residual-resistivity ratios ranging between 3 and 21. With the high-resolution techniques we have used, such samples are sufficiently clean to enable us to study in detail the magnetic contribution.

The magnetic properties of the rare-earth elements are largely determined by the interplay of the crystal field and the exchange interaction between the magnetic ions. When the ionic ground state is a singlet the exchange interaction and the crystal field act in

opposite directions, the former causing magnetic order and the latter tending to prevent it.[1] To study the competition between crystal field and exchange the alloy system $Tb_cY_{1-c}Sb$ is in many respects ideal. This system was first investigated by Cooper and Vogt,[2] who studied the magnetic susceptibility and the high-field magnetization. The concentration of the magnetic ions may be varied continuously between zero and unity without changing the crystal structure and the associated crystal field. The main effect of varying c is therefore to cause a change in the effective exchange interaction. In the dilute limit ($c \ll 1$) the crystal field is dominant, and the system is a Van Vleck paramagnet. When c increases, the effective exchange interaction increases relative to the crystal field, and when c exceeds 0.42 the alloy orders antiferromagnetically. The Néel temperature increases with increasing c and attains its biggest value (15.1 K) in pure TbSb.

In the dilute limit the individual magnetic ion has a nonmagnetic (singlet) ground state. The system therefore exhibits no Kondo behavior in the usual sense since the presence of an energy gap between the singlet ground state and the next excited states causes an exponential freezing out of the magnetic moment. We have been able to satisfactorily account for our observed resistivity by treating the interaction between the conduction electrons and the magnetic ions in the Born approximation, for both the dilute and the concentrated alloys. Within the Born approximation one may express the resistivity in terms of a weighted average over wave number $\vec{q}$ and frequency ω of the imaginary part of the ionic susceptibility function $\chi(\vec{q},\omega)$. Even though the system may not possess well-defined elementary excitations the resistivity is still given by a weighted average of $\mathrm{Im}\chi(\vec{q},\omega)$. This fact is particularly important for the spatially disordered magnetic systems we consider, since damping effects caused by the spatial disorder will be less important for the weighted average than for the elementary excitations themselves.

The aim of the present paper is twofold: First, to provide the detailed background for the previous results on the resistivity of the alloy system $Tb_cY_{1-c}Sb$, which have already been briefly reported.[3,4] Second, to extend these results to include the magnetically ordered phase of the alloy system.

The paper is organized as follows. Section II deals with the calculation of the resistivity and the magnetic susceptibility of the alloy $Tb_cY_{1-c}Sb$ within the random-phase approximation. The application to the resistivity of the paramagnetic phase of $Tb_cY_{1-c}Sb$ has already been made.[3,4] Here we extend the calculations to include also the magnetically ordered phase. In Sec. III we account for the techniques of crystal-growing, element analysis, and resistivity measurement, while the experimental results and the comparison to theory are discussed in Sec. IV. We conclude in Sec. V by discussing the theoretical model and the model parameters we have used to account for the experimental results.

II. RESISTIVITY AND MAGNETIC SUSCEPTIBILITY OF $Tb_cY_{1-c}Sb$

It is well known that the calculation of the electrical resistivity within the Born approximation may be formulated in terms of the imaginary part of the ion-ion susceptibility function. Such formulations have been used previously by many authors, e.g., in the context of transport calculations for liquid metals.[5,6] We shall sketch here and in the Appendix the derivation of the basic formula for the resistivity since an explicit expression which is readily applicable to magnetic systems does not seem to be available in the literature. The calculations rely on the spherical band approximation for the conduction electrons and are performed for a system of cubic symmetry in which case the resistivity is a scalar.

Application of the well-known variational principle[7] to the solution of the linearized Boltzmann equation allows one to put an upper bound on the resistivity ρ

$$\rho \leq \tfrac{1}{2}k_BT\left[\sum_{\vec{k}\sigma\vec{k}'\sigma'}(\phi_{\vec{k}}-\phi_{\vec{k}'})^2 P_{\vec{k}\sigma}^{\vec{k}'\sigma'} f^0(\epsilon_k)[1-f^0(\epsilon_{k'})]\right] \Bigg/ \left[\sum_{\vec{k}\sigma} e\vec{v}_k\cdot\hat{u}f^0(\epsilon_k)[1-f^0(\epsilon_k)]\phi_{\vec{k}}\right]^2 . \tag{2.1}$$

Here $P_{\vec{k}\sigma}^{\vec{k}'\sigma'}$ is the transition probability per unit time for the transition $\vec{k}\sigma\rightarrow\vec{k}'\sigma'$, given that the state $\vec{k}\sigma$ is occupied and the state $\vec{k}'\sigma'$ is unoccupied. f^0 is the Fermi function and $\hat{u}$ is a unit vector in the direction of the electric field. The electronic velocity is $\vec{v}_k=(1/\hbar)\partial\epsilon_k/\partial\vec{k}$. The electronic charge is denoted by e and $\epsilon_k=\hbar^2k^2/2m$. The function $\phi_{\vec{k}\sigma}$ appearing in Eq. (2.1) is an arbitrary trial function.

Throughout this work we employ a simple form for the electron-ion exchange interaction specified by the s-f Hamiltonian

$$\mathcal{H}_{sf}=-A(g-1)\sum_i \delta(\vec{r}-\vec{R}_i)\vec{J}_i\cdot\vec{s} , \tag{2.2}$$

where $\vec{r}$ ($\vec{R}_i$) is the position coordinate of the conduction electron (ion), $\vec{s}$ and $\vec{J}$ are the spin and total angular momentum operators ($s_z=\pm\frac{1}{2}$), A is the strength of their interaction, and g is Landé's factor for the $4f$ electrons. We also introduce the retarded

space-time susceptibility function per ion as

$$\chi^{\alpha\beta}(\vec{R},t) \equiv -i\langle[J_\alpha(\vec{R},t),J_\beta(0,0)]\rangle\Theta(t) \quad . \tag{2.3}$$

Here J_α is the α component of the total angular momentum operator in the Heisenberg representation, the bracket $\langle\ \rangle$ denotes thermal averaging, and $\Theta(t)$ is the usual step function.

We may express $P_{\vec{k}\sigma}^{\vec{k}'\sigma'}$ as follows:

$$P_{\vec{k}\sigma}^{\vec{k}'\sigma'} = \int d(\hbar\omega)\delta(\epsilon_{k'}-\epsilon_k-\hbar\omega) \times \int d^3q\ \delta(\vec{k}'-\vec{k}-\vec{q})\, w_\sigma^{\sigma'}(\vec{q},\omega) \quad , \tag{2.4}$$

where $w_\sigma^{\sigma'}(\vec{q},\omega)$ is the transition probability corresponding to a process in which an electron in spin state σ gains the momentum $\hbar\vec{q}$ and energy $\hbar\omega$ when going to the spin state σ'.

It is shown in the Appendix that

$$\sum_{\sigma'\sigma} w_\sigma^{\sigma'}(\vec{q},\omega) = A^2(g-1)^2 N_{\text{ion}} \times \frac{1}{e^{\hbar\omega/k_BT}-1}\,\text{Im}\,\text{Tr}\chi(\vec{q},\omega) \quad , \tag{2.5}$$

where $\text{Im}\,\text{Tr}\chi$ is the trace of the imaginary part of the ion-ion susceptibility function and N_{ion} is the number of ions per unit volume. The result (2.5) relies on the Born approximation for the interaction between the electrons and the ions.

When Eqs. (2.4) and (2.5) are introduced in Eq. (2.1) along with the standard trial function $\phi_k \propto \vec{k}\cdot\hat{u}$ we may perform some of the integrations removing the momentum δ function appearing in Eq. (2.4), with the final result

$$\rho = \rho_0 \int_0^1 d\left[\frac{q}{2k_F}\right]\left[\frac{q}{2k_F}\right]^3 \times \int \frac{d\Omega_{\hat{q}}}{4\pi}\int_{-\infty}^{\infty} d(\hbar\omega)\frac{\hbar\omega/k_BT}{\sinh^2(\hbar\omega/2k_BT)} \times \frac{1}{\pi}\,\text{Im}\,\text{Tr}\chi \quad , \tag{2.6}$$

where

$$\rho_0 = \frac{3\pi}{8}\frac{m}{e^2\hbar\epsilon_F}A^2(g-1)^2N_{\text{ion}} \tag{2.7}$$

and $\epsilon_F = \hbar^2k_F^2/2m$. The normalization constant ρ_0 has been chosen such that $\rho_0 J(J+1)$ is the high-temperature spin-disorder resistivity.

The magnetic contribution to the resistivity, Eq. (2.6) depends on the imaginary part of the trace of the magnetic susceptibility tensor, $\chi(\vec{q},\omega)$, and in this section we shall establish the model used for calculating $\chi(\vec{q},\omega)$ and thereby ρ in the particular case of $Tb_cY_{1-c}Sb$. Because of the (weighted) integrations of $\chi(\vec{q},\omega)$, with respect to the wave vector and the frequency, the calculation of ρ becomes less sensitive to the precise form of the response function. Hence, if the magnetic excitations of the system are reasonably well defined, the dependence of $\text{Im}\chi(\vec{q},\omega)$ on their finite lifetimes is eliminated, to a good approximation, when the integrations are performed. Accordingly, the RPA (random-phase approximation) calculation of $\chi(\vec{q},\omega)$ should be sufficiently accurate in most cases. If the two-ion couplings are of long range, produced by the indirect exchange mechanism, the ground state is close to the one determined by the molecular-field (MF) Hamiltonian, which we shall assume to be a valid approximation. For the dilute crystals in which some of the Tb ions are replaced randomly by the nonmagnetic Y ions, i.e., $c < 1$, we adopt the simplest procedure, the virtual-crystal approximation (VCA), as this is justified by the same two arguments presented above.

TbSb constitutes a remarkably simple magnetic system, as most of its properties are described by introducing only one single-ion and one two-ion parameter. It crystallizes in the NaCl structure, and because of the cubic point symmetry the operator equivalent of the crystal-field Hamiltonian takes the form[8]

$$V_c = B_4^0(O_4^0+5O_4^4)+B_6^0(O_6^0-21O_6^4) \quad , \tag{2.8}$$

when expressed in terms of the Stevens operators (the z axis being along a [001] direction). A number of experiments[2,9–11] all consistently indicate that B_6^0 is negligible in comparison to B_4^0, which is found to be positive and to lie between 6.6 and 8.0 mK. Here we shall use $B_4^0 = 7.98$ mK and $B_6^0 = 0$ which are the values obtained by Stutius[10] from his specific-heat measurements on $Tb_cY_{1-c}Sb$. In terms of the parameters, x and W, introduced by Lea, Leask, and Wolf[8] these values correspond to $x = -1$ and $W = -0.48$ K. The total angular momentum of the Tb ions, J, is equal to 6, and these crystal-field parameters yield a level scheme which have the Γ_1 singlet as ground state. The angular momentum operator, $\vec{J}$, couples the Γ_1 singlet only with the Γ_4 triplet which is also the lowest excited level lying at an energy, $\Delta = -30W = 14.4$ K above the ground state. The next excited level is also a triplet, $\Gamma_5^{(2)}$, with the excitation energy being approximately 30 K. The remaining part of the level scheme is at much higher energies, between 92 and 115 K and may be neglected below a temperature of ~50 K. Referring to the calculations of Lea, Leask, and Wolf[8] a closer examination of the relative variation of the lower levels and of their matrix elements with the $\vec{J}$ operator shows that the singlet-triplet-triplet system is not very sensitive to the value of B_6^0, and even a substantial change of x (from -1 to -0.7) would have a negligible effect on the paramagnetic susceptibility.

The frequency-dependent single-ion susceptibility, $\chi^{\alpha\beta}(\omega)$ is a sum of an inelastic and an elastic part

$$\chi_0^{\alpha\beta}(\omega) = \chi_{0,\text{inel}}^{\alpha\beta}(\omega) + \chi_{o,\text{el}}^{\alpha\beta}(\omega) \quad . \tag{2.9a}$$

Denoting the $2J+1$ eigenvalues of the MF Hamiltonian by E_i and the corresponding eigenstates by $|i\rangle$ then

$$\chi^{\alpha\beta}_{0,\text{inel}}(\omega) = \sum_{\substack{i,j \\ E_i \neq E_j}} \frac{\langle i|J_\alpha|j\rangle \langle j|J_\beta|i\rangle}{E_j - E_i - \hbar\omega}(p_i - p_j) \quad , \tag{2.9b}$$

where $p_i = e^{-\beta E_i}/\sum_j e^{-\beta E_j}$ is the population of the ith state ($\beta = 1/k_B T$). The elastic part contributes only at zero frequency, and is

$$\chi^{\alpha\beta}_{0,\text{el}}(\omega) = \delta_{\omega,0}\beta\left(\sum_{\substack{i,j \\ E_i = E_j}} \langle i|J_\alpha|j\rangle \langle j|J_\beta|i\rangle p_i - \langle J_\alpha\rangle \langle J_\beta\rangle \right) , \tag{2.9c}$$

where $\langle\ \rangle$ denotes a thermal expectation value. The MF value of ρ is obtained by introducing $\chi^{\alpha\beta}_0(\omega)$ in Eq. (2.6).

The integration with respect to the wave vector is trivial, and the frequency integral is calculated by replacing ω with $\omega + i\eta$ and taking the limit $\eta \to 0^+$. Then

$$\rho_{\text{MF}} = \rho_0 \sum_\alpha \left(\sum_{\substack{i,j \\ E_i \neq E_j}} \frac{\beta(E_i - E_j)p_i}{1 - \exp[-\beta(E_i - E_j)]} |\langle i|J_\alpha|J\rangle|^2 + \sum_{\substack{i,j \\ E_i = E_j}} |\langle i|J_\alpha|j\rangle|^2 p_i - (\langle J_\alpha\rangle)^2 \right) + \Delta\rho \quad . \tag{2.10a}$$

The last two terms in the large parentheses originate from $\chi^{\alpha\alpha}_{0,\text{el}}$, which is handled like the inelastic part by introducing an arbitrary small excitation energy. The last term, $\Delta\rho$, is a correction to the starting expression for ρ_{MF}. $\Delta\rho$ vanishes unless $\langle\vec{J}\rangle$ is nonzero, owing to an applied field or to an intrinsic magnetic ordering, and is produced by the static scattering potential

$$\Delta\mathcal{H}_{sf} = -(g-1)A \sum_i \delta(\vec{r} - \vec{R}_i)\langle\vec{J}_i\rangle \cdot \vec{s} \quad .$$

If $\langle\vec{J}_i\rangle$ is independent of i (or a periodic function of i) this potential only gives rise to a coherent scattering of the conduction electrons without any effect on ρ (as long as any superzone effect is excluded). This is the situation if $c = 1$. In the dilute case ($c < 1$) the nonmagnetic Y ions have to be included when the average potential is evaluated (here it is essential that the sites occupied by the Y ions are uncorrelated). The deviation of the potential from its mean value, on both the Tb and the Y sites, then gives rise to an incoherent scattering. The contribution, $\Delta\rho$, to the resistivity may be calculated directly (see Ref. 12) or may be written

$$\Delta\rho = \frac{1}{c}\rho_0[c(\langle\vec{J}\rangle - c\langle\vec{J}\rangle)^2 + (1-c)(\vec{0} - c\langle\vec{J}\rangle)^2]$$

(note, that ρ_0 is already proportional to the number of Tb ions, i.e., c), which becomes

$$\Delta\rho = \rho_0(1-c)\sum_\alpha (\langle J_\alpha\rangle)^2 \quad . \tag{2.10b}$$

Equations (2.10) are equivalent to the one used by Hessel Andersen *et al.*[3] in the case of $\langle\vec{J}\rangle = \vec{0}$. In the high-temperature limit ρ_{MF} reduces to the spin-disorder resistivity

$$\rho_{T\to\infty} = \rho_0 \sum_\alpha \langle J_\alpha^2\rangle = \rho_0 J(J+1) \quad . \tag{2.11}$$

The result for ρ_{MF} is useful at higher temperatures, or whenever the two-ion couplings are weak. In the case of TbSb the low-temperature resistivity is strongly modified by the two-ion interaction

$$\mathcal{H} = \sum_i V_c(i) - \tfrac{1}{2}\sum_{i,j} \mathcal{J}(\vec{R}_i - \vec{R}_j)\vec{J}_i \cdot \vec{J}_j \quad . \tag{2.12}$$

In the total Hamiltonian, $\mathcal{H}$, we include only a Heisenberg coupling [in accordance with the simple RKKY (Ruderman-Kittel-Kasuya-Yosida) theory], and neglect the possibility of (phonon-induced) quadrupole couplings.[13,14] The most characteristic phenomenon in the theory of singlet-ground-state magnetism (for a review see, e.g., Cooper[1]) is, that the presence of a two-ion coupling is not a sufficient condition for the occurrence of a magnetically ordered phase (the single-ion susceptibility stays finite in the limit of zero temperature), but the coupling has to exceed a threshold value. The RPA value of the susceptibility,[15–18] as derived from the two-ion interaction in Eq. (2.12), is

$$\chi^{\alpha\beta}(\vec{q},\omega) = \chi^{\alpha\beta}_0(\omega) + \mathcal{J}(\vec{q}) \times \sum_\gamma \chi^{\alpha\gamma}_0(\omega)\chi^{\gamma\beta}(\vec{q},\omega) \quad , \tag{2.13}$$

where $\mathcal{J}(\vec{q})$ is the Fourier transform of $\mathcal{J}(\vec{R}_i - \vec{R}_j)$. This is a general result valid in both the paramagnetic and ferromagnetic phases. In the case of cubic symmetry the single-ion susceptibility tensor is proportional to the unit matrix, $\chi^{\alpha\beta}_0(\omega) = \chi_0(\omega)\delta_{\alpha\beta}$, if the ground state is nonmagnetic, and we get from Eq. (2.13)

$$\chi^{\alpha\beta}(\vec{q},\omega) = \delta_{\alpha\beta}\frac{\chi_0(\omega)}{1 - \mathcal{J}(\vec{q})\chi_0(\omega)} \quad . \tag{2.14}$$

A second-order phase transition occurs at the temperature T_N, whenever $\chi^{\alpha\beta}(\vec{Q},\omega=0)$ diverges or

when

$$1 - \mathcal{J}(\vec{Q})\chi_0(\omega=0) = 0 \ , \tag{2.15}$$

where $\vec{Q}$ determines the periodicity of the magnetically ordered structure below T_N. TbSb is observed to order at $T_N = 15.1$ K in a type-II antiferromagnetic structure,[11,19] i.e., $\vec{Q} = (\pi/a)(1,1,1)$, where a is the lattice parameter. The magnetic moments are along a [111] direction, consistent with the positive sign of B_4^0. When $B_4^0 = 7.98$ mK is inserted in Eq. (2.15) one finds that $T_N = 15.1$ K corresponds to $\mathcal{J}(\vec{Q}) = 1.215$ K.

The magnetic unit cell in the antiferromagnetic phase is twice the crystallographic one, altering the $\vec{q}$-dependent susceptibility. The modification may be obtained by the following procedure. In each one of the two sublattices a separate coordinate system (x',y',z') is introduced, the z' axes being parallel to the magnetic moments (or the directions of the molecular fields) of either one of the two sublattices (the x' and y' axes being along the symmetry [110] and [112] directions). The components of $\mathcal{J}_i$ and of the susceptibility tensors, with respect to the two local coordinate systems, are denoted by primed indices, and we have

$$\vec{J}_i \cdot \vec{J}_j = J_{x',i}J_{x',j} + e^{-i\vec{Q}\cdot\vec{R}_{ij}}\,(J_{y',i}J_{y',j} + J_{z',i}J_{z',j})$$

and

$$\mathrm{Tr}\chi(\vec{q},\omega) = \chi^{x'x'}(\vec{q},\omega) + \chi^{y'y'}(\vec{q}+\vec{Q},\omega) + \chi^{z'z'}(\vec{q}+\vec{Q},\omega) \ .$$

The single-ion susceptibility, $\chi_0^{\alpha'\beta'}(\omega)$, is the same for all the ions, and equal to $\chi_0^{\alpha\beta}(\omega)$, when one of the primed coordinate systems is chosen to be the common (unprimed) one. After this transformation the conventional method[17,18] is applicable. The cubic point symmetry allows a simplification of the final expressions which is utilized by introducing the susceptibilities defined in terms of $J^{\pm}$ instead of J_x and J_y.[18]. The results are

$$\chi^{zz}(\vec{q},\omega) = \frac{\chi_0^{zz}(\omega)}{1 - \chi_0^{zz}(\omega)\mathcal{J}(\vec{q})} \ , \tag{2.16a}$$

which is the same expression as in the paramagnetic case, whereas

$$\chi^{xx}(\vec{q},\omega) = \chi^{yy}(\vec{q},\omega) = \frac{\chi_0^{+-}(\omega) + \chi_0^{-+}(\omega) - \chi_0^{+-}(\omega)\chi_0^{-+}(\omega)\,\mathcal{J}(\vec{q}+\vec{Q})}{4 - [\chi_0^{+-}(\omega) + \chi_0^{-+}(\omega)][\mathcal{J}(\vec{q}) + \mathcal{J}(\vec{q}+\vec{Q})] + \chi_0^{+-}(\omega)\chi_0^{-+}(\omega)\mathcal{J}(\vec{q})\mathcal{J}(\vec{q}+\vec{Q})} \ , \tag{2.16b}$$

where $\chi_0^{+-}(\omega)$ is equal to $[\chi_0^{-+}(-\omega)]^*$. In the paramagnetic phase, $T > T_N$, $\chi_0^{+-}(\omega) = \chi_0^{-+}(\omega) = 2\chi_0^{zz}(\omega)$, by which the right-hand side of Eq. (2.16b) is reduced to be equal to $\chi_{zz}(\vec{q},\omega)$. The single-ion and thus the $\vec{q}$-dependent susceptibilities are continuous functions of T, also at T_N. In the ordered phase, $T < T_N$, a reversal of the magnetization [which affects the single-ion susceptibilities only by interchanging $\chi_0^{+-}(\omega)$ and $\chi_0^{-+}(\omega)$] has no effect on ρ, implying that $\rho(T)$ depends linearly on $T_N - T$ in the limit $T_N - T \to 0^+$ as

$$\rho(T_N) - \rho(T) \propto (\langle J_z \rangle)^2 \propto T_N - T \ . \tag{2.17}$$

The $\vec{q}$ dependence of $\chi^{\alpha\alpha}(\vec{q},\omega)$, introduced by the Eqs. (2.14) and (2.16), is simplified by use of the approximate expression

$$\mathcal{J}(\vec{q}) = \mathcal{J}[\cos(q_x a) + \cos(q_y a) + \cos(q_z a)] \ , \tag{2.18a}$$

which implies

$$\mathcal{J}(\vec{q}+\vec{Q}) = -\mathcal{J}(\vec{q})$$

and

$$\mathcal{J}(\vec{Q}) = -3\mathcal{J} \ . \tag{2.18b}$$

Accounting only for the coupling between the six next-nearest neighbors, we have kept the number of parameters at a minimum. From their inelastic neutron experiment on TbSb Holden *et al.*[9] derived that the nearest-neighbor interaction should also be of some importance. However, the approximate expression, Eq. (2.18), retains the most characteristic features of a more realistic $\mathcal{J}(\vec{q})$. In their analysis of the magnetization measurements on $Tb_cY_{1-c}Sb$, Cooper and Vogt[2] also used this simplification.

In the present calculations the RPA value of $\chi(\vec{q},\omega)$ is fixed alone by the two parameters, B_4^0 and $\mathcal{J}(\vec{Q})$, besides the additional one characterizing the dilute crystals, namely, c. If c is less than one the only modification of the equations above is the introduction of the c-dependent exchange coupling

$$\mathcal{J}_c(\vec{q}) = c\mathcal{J}_{c=1}(\vec{q}) \ . \tag{2.19}$$

The use of the virtual-crystal (VC) approximation means that the random replacement of the fraction $1-c$ of the Tb ions with the nonmagnetic Y ions only introduces a uniform scaling of the two-ion interaction. We expect an intrinsic c dependence of the parameters to be small. Except for the $4f$ electrons the electronic structures of the Tb ions and of the Y ions are very similar, and the lattice parameter is

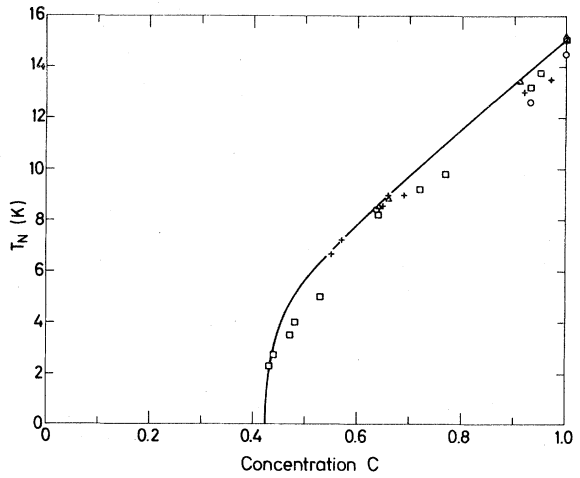

FIG. 1. Experimental transition temperatures T_N of $Tb_cY_{1-c}Sb$ determined from measurements of susceptibility, □ (after Ref. 2); specific heat, ○ (after Ref. 10); neutron diffraction, Δ (after Ref. 11); and electrical resistivity, +. The solid line is the molecular-field value of T_N.

nearly independent of c (ranging[2] from 6.165 Å in YSb to 6.180 Å in TbSb, which variation only affects B_4^0 by 1.2% within a point-charge model). In the previous calculation of ρ in the paramagnetic phase[4] we introduced in addition a concentration-dependent effective lattice parameter, which resulted in a scaling of the wave vector appearing in $\mathcal{J}_c(\vec{q})$. This procedure is abandoned here since it has no real justification (the fit is almost unaffected by this change).

The parameters $B_4^0 = 7.98$ mK and $\mathcal{J}_{c=1}(\vec{Q}) = 1.215$ K, used in the present calculations, account reasonably well for most of the observed magnetic properties of the $Tb_cY_{1-c}Sb$ system.[2,9-11]

In pure TbSb the zero-temperature moment, $\langle J_z\rangle_{T=0}$, is calculated to be 5.15, which is close to the saturation value $J=6$ and in fair agreement with the experimental results of Cable *et al.*[11] ($\langle J_z\rangle_{T=0}=5.22$) and of Child *et al.*[19] ($\langle J_z\rangle_{T=0}=5.45$) both obtained by neutron diffraction. Because the ground state of the crystal-field Hamiltonian is a singlet the transition temperature, calculated by the use of Eq. (2.15) and (2.19), does not scale linearly with c. In Fig. 1 we show T_N versus c compared with the values obtained by various experiments. The good agreement yields an independent check on our parameters, or may, alternatively, be used as a justification of the VC approximation. At $c=0.42$ T_N is found to vanish, meaning that the singlet-ground-state system is subcritical when $\mathcal{J}(\vec{Q})$ is smaller than $0.42\mathcal{J}_{c=1}(\vec{Q}) = 0.51$ K. This critical value of the concentration of Tb ions is concordant with experiments as no magnetic ordering has been observed for c less than 0.42.

The $\vec{q}$-dependent susceptibilities, Eqs. (2.14) or (2.16), are now introduced in the expression for ρ. The frequency integral in Eq. (2.6) may easily be brought into an analytic form in the paramagnetic case, when only the singlet-triplet-triplet part of the level scheme is considered (we shall not state the result here, but refer to Ref. 15). In the ordered phase the level scheme is too complicated to allow an analytic approach. Instead the eigenvalue equation corresponding to $\chi^{zz}(\vec{q},\omega)$ was transformed into a Hermitian form and solved numerically. In the case of $\chi^{xx}(\vec{q},\omega)$ the eigenvalue equation is not Hermitian, and here we applied the numerical method also introduced by Buyers *et al.*,[18] in which ω is replaced by $\omega+i\eta$, but instead of taking the limit $\eta\to 0$, η is retained as a finite quantity throughout the calculations (we have used $\eta\cong 5$ mK). The elastic contributions [below T_N only $\chi^{zz}(\vec{q},\omega)$, Eq. (2.16a) gives rise to such contributions], may be written explicitly

$$\sum_\alpha \frac{1}{4}\lim_{\epsilon\to 0}\int_{-\epsilon}^{\epsilon} d(\hbar\omega)\frac{\beta\hbar\omega}{\sinh^2(\beta\hbar\omega/2)}\frac{1}{\pi}\mathrm{Im}\chi^{\alpha\alpha}(\vec{q},\omega) = \sum_\alpha\left(\sum_{\substack{i,j\\ E_i=E_j}}|\langle i|J_\alpha|j\rangle|^2 p_i - \langle J_\alpha\rangle^2\right)$$

$$\times\{[1-\chi^{\alpha\alpha}_{0,\mathrm{inel}}(0)\,\mathcal{J}(\vec{q})][1-\chi^{\alpha\alpha}_0(0)\,\mathcal{J}(\vec{q})]\}^{-1}+\frac{\Delta\rho}{\rho_0}\ , \qquad (2.20)$$

including the effect $\Delta\rho$ due to the static potential scattering. $\Delta\rho$ is not affected by the two-ion coupling between the Tb ions and is given by Eq. (2.10b). In the limit of $T\to 0$ the inelastic contributions vanish and of the elastic terms, Eq. (2.20), only $\Delta\rho/\rho_0$ survive implying a magnetic contribution to the residual resistivity determined by

$$\frac{\rho_{T=0}}{\rho_{T\to\infty}} = \frac{(1-c)(\langle J_z\rangle_{T=0})^2}{J(J+1)}\ . \qquad (2.21)$$

The calculated value of this ratio as function of c is shown in Fig. 2.

The final integration with respect to $\vec{q}$ has been done numerically where we summed over 5000 points in the Brillouin zone. Actually, it turned out that the quite small value of k_F, obtained by the fitting procedure (see Sec. IV) allowed the use of a spherical interpolation calculation as the integrand is only weakly dependent of the solid angle $\Omega_{\hat{q}}$.

III. EXPERIMENTAL TECHNIQUE

The $Tb_cY_{1-c}Sb$ crystals used in our resistivity measurements have been made from metals of the

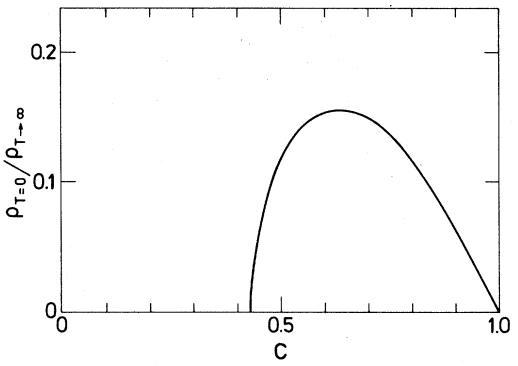

FIG. 2. Virtual-crystal calculation of the magnetic residual resistivity of $Tb_cY_{1-c}Sb$, normalized to the high-temperature saturation value $\rho_{T\to\infty}$.

highest commercially available purity, i.e., for Tb: 99.9%, Y: 99.9%, and Sb: 99.999%. The crystal growing is performed in a two-step process. (A more thorough account of the process of crystal growing and the methods of analysis discussed below may be found in Ref. 12.) First a polycrystalline powder is formed by prereacting small turnings of the constituents for two weeks in evacuated (10^{-5} Torr) quartz tubes with temperatures increasing from 125 °C to about 700 °C. In an evacuated pressure cell the polycrystalline powder is exposed to a pressure of 70 atm. and formed into a pellet which for the final reaction is placed in an evacuated (10^{-4} Torr) molybdenum crucible. The formation of single crystals is made in an oven at approximately 2100 °C during an eight to ten day period. The crystallization may take place either by sublimation or recrystallization, or both simultaneously, depending presumably on the size of the temperature gradients over the crucible. In the sublimation process the crystals are formed at the (colder) top of the crucible, whereas in recrystallization they appear at the bottom.

The single crystals are easily cleaved from the bulk of the sample to form small rectangular prisms with faces congruent to the crystallographic (100) planes of the rocksalt crystal structure. Just after cleaving they appear with a shiny metallic surface, which becomes dull and dark after a few days exposure to the atmosphere. The interior, however, stays unaffected as may be seen by renewed cleavings. The sample size is typically 3 mm in length and 0.5 mm^2 in the base area.

In the mixed crystals of $Tb_cY_{1-c}Sb$ the Tb and Y ions are assumed to substitute one another in a random way. The similarity in ionic radii of Tb and Y and the very small variation in lattice constant throughout the series support this belief. Measurements of specific-heat,[10] susceptibility,[2] and the present resistivity investigations, however, disclose concentration gradients in the samples and deviations from the nominal (as predestinated in the crystal processing) Tb concentrations. The samples used in the specific-heat and the susceptibility measurements are composed of several single crystals. The concentration inhomogeneities, which in particular are revealed in the broadening of the specific-heat peaks at the ordering temperatures, may therefore result from gradients within the single crystals or, as suggested by the differences in the process of crystal growing, among them. The high-temperature slopes of the inverse susceptibilities may be used to determine the

TABLE I. Concentration analysis of $Tb_cY_{1-c}Sb$.

Nominal c (%)	Neutron activation $c \pm 2$ (%)	Electron microprobe $c \pm 3$ (%)	X-ray fluorescence $c \pm 3$ (%)	Susceptibility c (%)
0		0		
5	6	6	5	5
20	24	27	23	22
30	36	33	48	31
38	45	46	45	40
40	46			43
45	48	53	55	
50	55	59	58	53
55	57	65	70	
60	69		76	64
70	65	74	82	72
80	66	73		77
90	92	93	88	
95	97	95	98	95
100	100	100		

Tb concentrations. In Table I we have shown the Tb concentrations obtained by Cooper and Vogt[2] from their susceptibility measurements. Although each result represents an average over many single crystals it is seen that their values may deviate from the nominal concentrations. More distinct deviations may be found in our single-crystalline resistivity measurements where the ordering temperatures in some cases are far from predictions based on the nominal concentrations.

To clarify the concentration problems the crystals have been subjected to four different examinations: Neutron activation, electron microprobe, x-ray fluorescence, and metallographic analysis.

The samples actually used in our resistivity measurements have been investigated only by neutron activation analysis. The results given in Table I represent the relative atomic percent of the Tb and Sb content as compared to a TbSb standard. Although the samples have not been destroyed during the analysis the accuracy is indicated to be ±2% in the absolute value. This is obtained by an extension of the standard method in which the absorption effects have been corrected for by analysis of two essentially different γ_{Tb} lines. Rather large deviations from the nominal concentrations are measured, especially for the sample with nominal concentration $c=0.80$. It is measured to be $c=0.66$ which agrees with the transition temperature observed in the resistivity measurements. Note also that the samples with nominal concentrations betwee 60 and 80% all turn out to have the same Tb to Y ratio of 2:1. Apart from samples with nominal concentrations $c=0.70$ and 0.80 the results of the analyses proved to give larger c values. Although different crystals are used in the other methods of analysis the same general tendency is obtained. It should be mentioned in this connection that in many cases the crystals come from the same batch.

In the x-ray fluorescence analysis[20] the samples are dissolved in order to avoid absorption effects. The intensities of characteristic fluorescence lines from the solutions are compared to standard solutions of pure Tb, Y, and Sb. The accuracy is indicated to be ±3%. In some cases the results do not agree with those obtained by the other investigations. It has not been possible to explain these larger discrepancies.

The electron microprobe technique[20] allows for very detailed analysis of the homogeneity. Also it is possible to obtain the absolute concentrations by use of a complex correction method.[21] In the present case the electron beam generating the characteristic x-ray lines has a diameter of 0.5 μm. The analysis revealed no gradients in the Tb and Y content over the samples. This contrasts earlier investigations[2] with the same technique where the inhomogeneities over the samples in the worst cases amounted to 2% in absolute values. They could be removed by annealing the samples at 1400 °C for some days and may have resulted from insufficient reaction time in the early days of the crystal processing. For the absolute Tb concentrations, accurate within ±3%, we have in Table I given the Tb to Sb ratio.

The advisability of making microprobe analysis on the samples is emphasized by the occasional observation of inclusions containing Tb_3Sb_4. By metallographic examinations the areas of the largest inclusions in these crystals were found and Tb_3Sb_4 islands as large as 60-μm diam were observed.

In conclusion it should be mentioned that none of the methods of analysis is able to detect the content of oxygen. From the process of crystal growing, especially in the prereaction, contamination with oxygen cannot be excluded and may give rise to small undiscovered islands of Tb and/or Y oxide.

The electrical resistivity measurements have been performed in a standard liquid-^{4}He cryostat. A stainless-steel tube immersed in the He bath is evacuated to isolate the pot of the sample holder thermally from the bath. The pot is heated externally and the heat is conveyed to the sample via He exchange gas in the pot. The thermal contact between the sample and the thermometer is established via copper joints and is therefore much better than to the heater and the bath. This allows for rapid change of temperature without conflicting the isothermal conditions.

The temperature is stabilized to within 0.01 K with a THOR-Cryogenics Ltd., model 3010 temperature controller (Allan and Bradley carbon sensor below 40 K, a platinum resistor above). The thermometer consists of an Au(+0.03 at.% Fe) versus chromel thermocouple with the fixed point in liquid nitrogen. The thermovoltage generated at liquid-He temperature is approximately 1 mV and the thermopower is 10-15 μV/K. In order to measure the temperature to within 0.01 K a compensating system (accuracy better than 0.1 μV) is used. The uncompensated signal corresponding to approximately 1 K is recorded.

The electrical resistivity is measured by a standard four-point dc method. Copper leads of 0.2-mm diam are spot welded to the crystal in a configuration where boundary conditions are of no consequence.[22] However, with a distance of approximately 1 mm between the voltage leads, the uncertainty in the absolute value of the resistivity may be as large as ±20%. An attempt to reduce the diameter of the voltage leads conflicted the demand of mechanical and electrical stability.

The excitation current of 10 mA is supplied by a constant current source, stable within 5×10^{-4} over a day. It is kept as low as possible without affecting the resolution set by the voltage detecting system. It is about a factor of 10 below the limit where deviations from Ohm's law may be seen. Possibly, the deviations thus observed may originate from self-

heating at the contact points of the current leads which have a resistance of approximately 50 mΩ each. The thermovoltages introduced by asymmetrical joule heating and in the voltage loop in general are compensated by reversing the current. It should, however, be mentioned that the thermovoltages generated by Peltier effect are reversed with the current. They may only be avoided by having low-excitation currents and good thermal anchoring at the endpoints of the crystal.

The voltage detecting system consists of a Keithley Instruments model 148 dc nanovoltmeter, amplifying the signal 10^4 or 10^5 times, and a Hewlett-Packard dc differential compensating voltmeter model 3420*B*. Like the case of temperature recording the sample voltage is compensated for the first two or three digits and the last two recorded. The sensitivity of the system is limited by the Johnson noise which at room temperature amounts to 1 nV peak to peak and by the resolution of the chopper amplifier in the nanovoltmeter, being 1 nV also. The linearity of the nanovoltmeter and the stability of the differential compensating voltmeter give an estimated accuracy of approximately $1:10^4$. With a characteristic sample

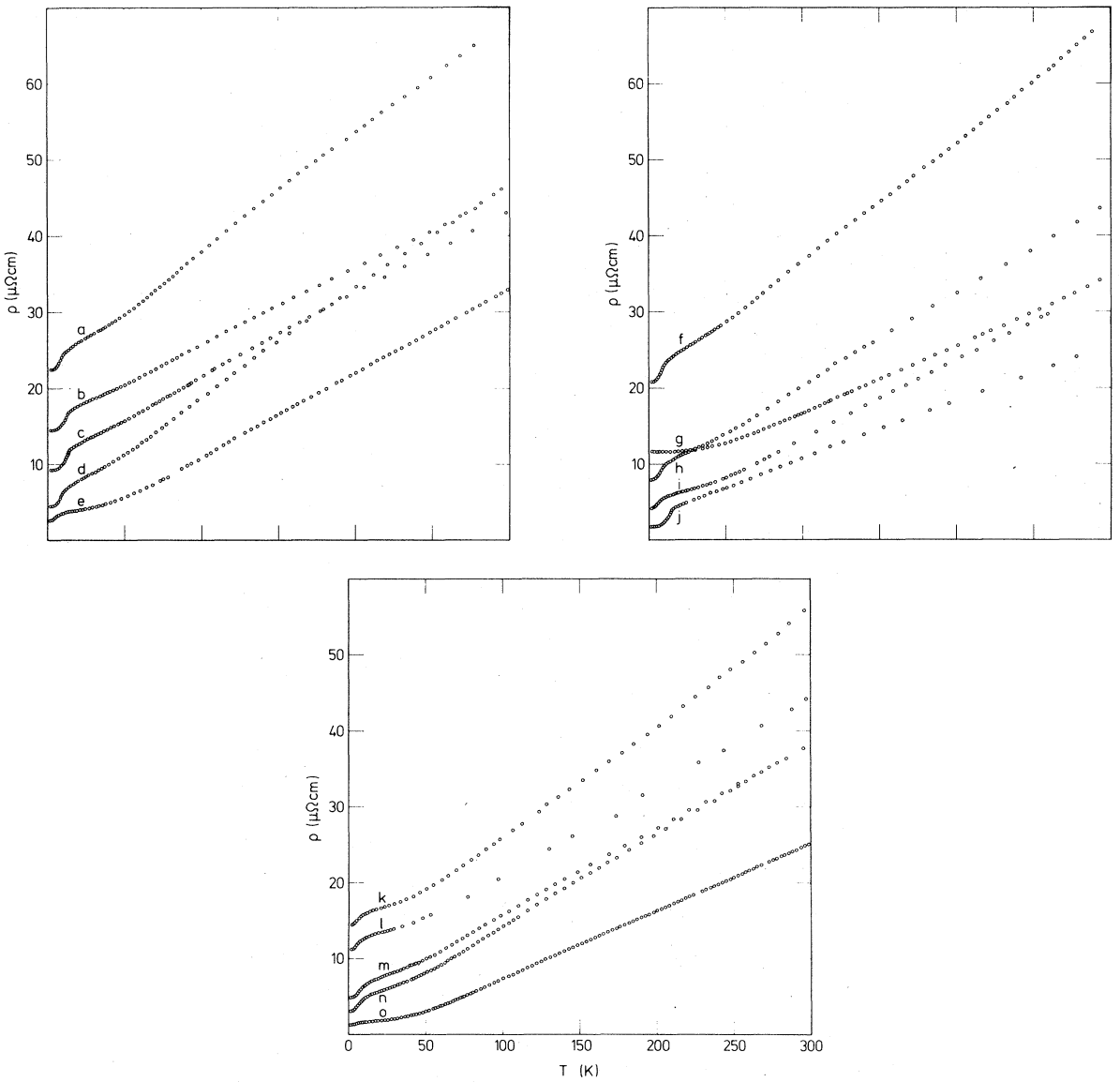

FIG. 3. Electrical resistivity measurements on single crystalline $Tb_cY_{1-c}Sb$ with the current in the [100] direction. The results are displayed in three figures for clarity. The latin letters refer to the following concentrations: *a*, $c=0.69$; *b*, $c=0.92$; *c*, $c=0.97$; *d*, $c=0.65$; *e*, $c=0.24$; *f*, $c=0.66$; *g*, $c=0$; *h*, $c=0.57$; *i*, $c=0.46$; *j*, $c=1.00$; *k*, $c=0.36$; *l*, $c=0.45$; *m*, $c=0.55$; *n*, $c=0.48$; *o*, $c=0.06$.

resistance of 1 mΩ at low temperatures and the excitation current of 10 mA, this is also the resolution obtained by the nanovoltmeter.

IV. EXPERIMENTAL RESULTS AND THEIR INTERPRETATION

We have measured the electrical resistivity of 15 samples of $Tb_cY_{1-c}Sb$ as a function of temperature from 1.5 to 300 K over the whole range of concentration c. The results are shown in Fig. 3, displayed in three separate figures for clarity. All measurements have been performed with the current in the [100] direction. The resistivities are obtained from the measured voltages using the geometry of the crystal and the positions of the potential leads. As discussed in Sec. III this procedure introduces a quite large uncertainty in the absolute value of the resistivity, which is reflected in the variations of the high-temperature slopes for the resistivity curves in Fig. 3. In order to check whether the scatter in the results is due only to their uncertainties or whether any systematic dependences are involved we have analyzed the results carefully. No correlations could be detected between the concentration on one side and the residual resistivities, the high-temperature slopes of the resistivity, or the quality of the crystals on the other. Also there are no correlations between the quality of the crystals and the high-temperature slopes. As a measure for the quality we use the resistivity ratio $\rho_{300}/\rho_{1.5}$, which is not affected by the large uncertainties in the geometrical factor.

Both the magnitude of the resistivity and its linear increase with temperature at high temperatures indicate the metallic nature of the alloy systems. A typical value of the measured high-temperature slopes is 100 nΩ cm K^{-1} which is comparable to that of pure Tb metal. The absence of correlation between the quantities mentioned above gives further evidence for the crystals being metals and not impurity-doped small-gap semiconductors or semimetals (the rare-earth nitrides are know to be semiconductors).

In the metals the linear dependence of the resistivity on temperature is associated with the scattering of conduction electrons against lattice vibrations at temperatures comparable to or larger than a typical phonon frequency. A variation in the slope with concentration could result from a change in the effective number of conduction electrons, in the lattice vibrational spectrum or in the electron-lattice coupling. The high-temperature slopes in Fig. 3 show no evidence for any systematic variation with c and the largest deviation from the mean value of 117 nΩ cm K^{-1} amounts to 30% which is close to the estimated absolute uncertainty of 20%. This result indicates that the scatter in the absolute values of the high-temperature slopes is due to the experimental uncer-

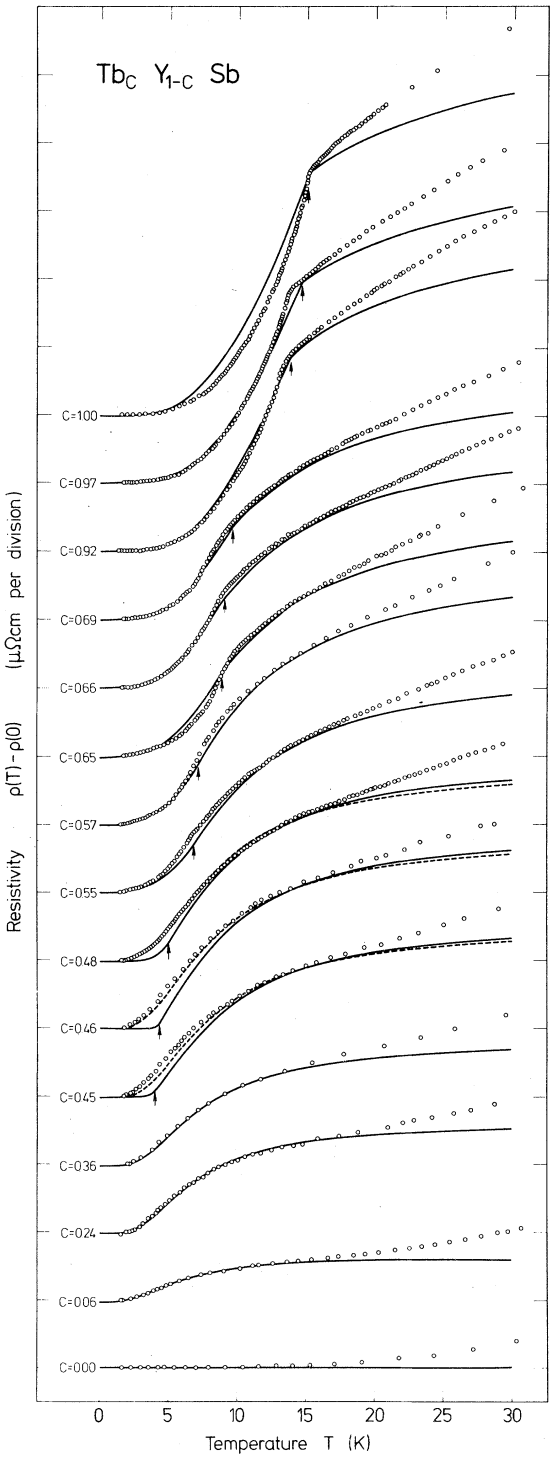

FIG. 4. Low-temperature resistivity of $Tb_cY_{1-c}Sb$. For each concentration c the residual resistivity has been subtracted and the base line has been arbitrarily chosen. The solid line is the resistivity calculated as described in Sec. II. The dashed lines are results assuming no magnetic ordering for the concentrations $c = 0.45$, 0.46, and 0.48. In all cases the theory has been fitted to the experimental data at 15 K. The arrows indicate the molecular-field transition temperatures T_N.

tainties only. In order to reduce the influence of the scatter in the absolute results we scale the measured resistivity for the different crystals such as to get high-temperature slopes equal to the mean value. That the high-temperature slopes should be independent of c is also a consequence of assuming an Einstein model for the lattice spectrum with equal force constants for the independent Tb and Y oscillators.

In Fig. 4 we present our experimental results in the low-temperature regime from 1.5 to 30 K together with the results of the model calculation described in Sec. II. For the sake of clarity the base lines have been shifted by an arbitrary amount for each alloy.

The total resistivity originates in ordinary elastic impurity scattering, electron-phonon scattering, and the scattering against the excitations associated with the magnetic ions. The total resisitivity is not simply a sum of the resistivities for each scattering mechanism considered separately (deviations from Matthiessen's rule). However, when ordinary impurity scattering dominates we are able to take into account the deviations from Matthiessen's rule within our theoretical model by separating the total resistivity in three terms

$$\rho = \rho_{\text{res}} + \rho_{\text{ph}}(T) + \rho_m(T) \ ,$$

where ρ_{res} is the temperature-independent residual resistivity resulting from ordinary electron-impurity scattering, while ρ_{ph} and ρ_m are the additional contributions to the resistivity associated with scattering against phonons and magnetic excitations, respectively.

In all crystals except for YSb ($c = 0.00$), in which only electron-phonon scattering contributes to the temperature dependence, the magnetic scattering dominates the scattering against lattice vibrations below 15 K. When we fit our calculated ρ_m to the experimentally determined $\rho - \rho_{\text{res}}$ at 15 K the remaining resisitivity contribution is qualitatively similar to the electron-phonon resistivity of YSb, in which the temperature variation is seen to be very small below 15 K. We have therefore chosen $T = 15$ K as a fitting temperature for the comparison between our experimental results and our calculated resistivity values.

To make a detailed comparison between experiment and the free-electron calculations of Secs. I–III one needs a value of the Fermi wave vector k_F. Various aspects of the experimental results suggest k_F to be small. First of all, the resistivities in the paramagnetic phase exhibit a slower rise towards saturation the larger the concentration. The formation of bands from crystal-field levels, introduced by the antiferromagnetic two-ion interaction, increases the energy of excitations at small wave vector and decreases the energy of excitations at large $\vec{q}$. Consequently, the cutoff at the maximum wave-vector transfer $2k_F$ implies a slower rise towards saturation if $2k_F$ is small. This effect increases with the concentration because the dispersion increases with the magnitude of the effective two-ion interaction. Second, there is no experimental evidence for superzone effects, which may occur at a magnetic phase transition, if the magnetic unit cell differs from the crystallographic one, corresponding to $\vec{Q} \neq 0$ in the notation of Sec. II. A necessary condition for the superzone effect to appear is that the wave vector $\vec{Q}$ should connect points at the Fermi surface. Since superzone effects are not observed, we expect $2k_F$ to be smaller than $|\vec{Q}| = \sqrt{3}\pi/a$. The best overall agreement was obtained by choosing $2k_F = 3\pi/4a$ after several attempts with values of $2k_F$ in the range from $\pi/2a$ to π/a. The result of this calculation is shown as the solid lines in Fig. 4.

The overall agreement is very satisfactory considering the large amount of data and the use of essentially only two adjustable parameters. We have used k_F as a fitting parameter common to all concentrations, but fitted the constant ρ_0 in Eq. (2.6) independently for each concentration. In Fig. 5 we exhibit the concentration dependence of ρ_0 which within our model should be proportional to c. The standard deviation of ρ_0/c from a constant value amounts to 15%, which is more than the 5–8% expected from the uncertainty in the absolute resistivity values after one has performed the high-temperature scaling described above. This discrepancy, which is barely significant, is the only indication we have found for a systematic variation of the electronic properties of the $\text{Tb}_c\text{Y}_{1-c}\text{Sb}$ alloy systems with the concentration of magnetic ions. There are no more free parameters entering our fit, since the magnetic susceptibility is calculated with crystal-field parameters given by other experiments[10] and an exchange constant determined from the ob-

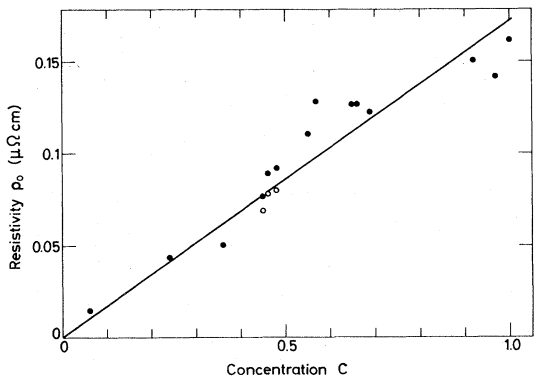

FIG. 5. Concentration dependence of the parameters ρ_0 as determined from Fig. 4. Solid circles correspond to solid lines in Fig. 4, open circles to dashed lines. The straight line, corresponding to the theoretical prediction of Eq. (2.7), is obtained from a least-square fit to the solid circles.

served ordering temperature of TbSb.

In the temperature range below 15 K the agreement between experiment and theory is excellent for the samples which are not expected to order ($c < 0.42$). In the concentration range where the molecular-field calculations lead to ordering at the temperature indicated by an arrow in Fig. 4 the agreement is in some cases less satisfactory. For the ordered phases one must keep in mind that the theoretical results are very sensitive to the value of $\langle J_z \rangle$ and hence to the accuracy by which the molecular-field calculations reproduce the experimental values of $\langle J_z \rangle$. For the concentrations $c = 0.45$, 0.46, and 0.48 the contribution $\Delta\rho$ from the static potential scattering may give rise to large errors. $\Delta\rho$ is zero in the paramagnetic phase but increases as the square of the sublattice magnetization. From Fig. 2, which shows the relative values $\Delta\rho/\rho_{T\to\infty}$ at zero temperature, it may be seen that just above the critical concentration ($c = 0.42$) the magnetic residual resistivities should be large in disagreement with experiments. This is presumably due to the inadequacy of the virtual-crystal and molecular-field determination of the transition temperature close to the critical concentration. To consider the possibility that these crystals do not order, we have extended the resistivity calculations to zero temperature assuming the ground state to be nonmagnetic. The results, which are shown as dotted lines in Fig. 4, give a much better agreement with experiment. The corresponding values obtained for ρ_0 are shown in Fig. 5 as open circles.

In the concentration range $0.55 \leq c \leq 0.69$ there is likely to be some discrepancy connected with our use of the virtual-crystal approximation which is better justified in the high- and low-concentration limits. We also mention that our results show that it is difficult to extract a precise value of the transition temperature from resistivity measurements. This is because the rapid decrease in resistivity normally seen below a transition temperature has already started above the transition due to the thermal depopulation of the excited states which causes the temperature dependence of the single-ion resistivity.

For the three most concentrated samples, where the transition temperatures are easily identified in the experiments we may still find some deviations from the theoretical predictions. Apart from minor discrepancies between the molecular-field predictions of T_N and the experimental values (largest for $c = 0.92$) we also find too steep a descent in the experimental data below T_N when compared with the calculations. In Sec. II we argued that the resistivity should change below T_N just like $\langle J_z \rangle^2$ which within molecular-field theory is proportional to $T_N - T$. However, the actual sublattice magnetization in the critical region, as determined from neutron scattering experiments, has a much faster temperature variation given by

$$\langle J_z \rangle^2 \propto (T_N - T)^{2\beta} ,$$

since the measured exponents are $\beta \simeq 0.2$ for TbSb and $\beta \simeq 0.35$ for the diluted systems.[23] The inaccuracy of the molecular-field ground state is therefore the most important reason for the discrepancy below T_N.

We also remark that long-range critical fluctuations in the case of antiferromagnetic ordering only influence the resistivity if, as with the superzone effect, the wave vector $\vec{Q}$ connects points at the Fermi surface.

At temperatures higher than 15 K the experimental and theoretical curves deviate increasingly. This is to be expected from the presence of electron-phonon scattering. At small concentrations the deviations correspond closely to the temperature-dependent resistivity of YSb, which is entirely due to electron-phonon scattering. At higher concentrations the deviations become relative larger (at a fixed temperature). This trend is quite plausible since the mass of a Tb ion is nearly twice that of a yttrium ion. The effective Debye temperature must therefore decrease when c increases, leading to an increase in the low-temperature electron-phonon resistivity as observed experimentally.

V. CONCLUSION

In this work we have made a detailed study of the temperature-dependent resistivity of a series of alloys, in which the concentration of magnetic ions may be varied continuously. The dilute alloys are Van Vleck paramagnets, but they order antiferromagnetically when the concentration of the magnetic ions exceeds about 40% of its maximum value. Over the entire range of concentrations we have been able to account satisfactorily for that part of the temperature-dependent resistivity which is due to magnetic scattering. Within the Born approximation for the electron-ion scattering the resisitivity depends on a certain weighted average of the ion susceptibility function, which we calculate within the random-phase approximation supplemented by a mean-field, virtual-crystal treatment of the magnetically ordered ground state.

The detailed comparison in Sec. IV between experiment and theory suggests that the RPA approximation for the excitations is quite adequate. Our greatest simplification concerns the conduction-electron band structure, which we have treated in a spherical model characterized by a Fermi wave vector k_F. In the comparison with experiment k_F was considered an adjustable parameter common to all alloys (independent of c). Apart from determining the overall scale of the resistivity the magnitude of k_F has a decisive influence on its temperature dependence in the more concentrated alloys, since $2k_F$ acts as a cutoff for the wave vector of the magnetic exci-

tations involved in the scattering. The comparison in Sec. IV shows that the temperature-dependent resistivity for the whole alloy series can be understood in terms of basically two parameters, the Fermi wave vector k_F and the scale factor ρ_0 for one particular concentration. If ρ_0 is treated as an adjustable parameter for each concentration, one finds that ρ_0/c to a good approximation is equal to a constant, as predicted by the simple model.

In addition there are two other parameters entering the theory: The crystal-field parameter B_4^0 for a single ion and the exchange constant $\mathcal{J}(\vec{Q})$ characterizing the ordered state. The parameter B_4^0 was obtained from specific-heat measurements[10] and used together with the observed Néel ordering temperature in TbSb to determine $\mathcal{J}(\vec{Q})$. In the free-electron model the constant ρ_0 is determined by k_F and the electron-ion exchange constant A according to Eq. (2.7). If we use the values of our fit parameters k_F and ρ_0 to determine the electron-ion exchange constant we obtain a reasonable value for A, but its inferred magnitude will of course change, if the conduction electrons are characterized by an effective mass that differs from the free-electron value. The main feature of our model for the electronic energy bands is the smallness of the Fermi wave vector which means that only magnetic excitations with rather small wave vectors are involved in the scattering. Other than that the model is too crude to allow any definite conclusions to be drawn for the magnitude of the electron-ion exchange constant.

Finally we remark that we have considered exchange scattering processes as being the sole cause for the characteristic low-temperature behavior of the electrical resistivity in the present alloy series. In the related rare-earth alloy TmSb it appears necessary[14] to take into account the scattering of the conduction electrons from the $4f$ quadrupole charge distribution as well. The reason, why this process is unimportant relative to the exchange in TbSb, is the magnitude of $g-1$ in the two systems. Since $g-1$ is $\frac{1}{2}$ for Tb^{3+} ions and only $\frac{1}{6}$ for Tm^{3+} ions the exchange contribution dominates the quadrupolar term in TbSb but not in TmSb. One must therefore be careful in applying the conclusions obtained from this study of the Tb-alloy system to other rare-earth systems without consideration of possible additional scattering contributions.

ACKNOWLEDGMENTS

It is a pleasure to thank K. Heydorn, Isotope Laboratory, Risø, Denmark for performing the neutron activation analysis, R. Gubser, Institut für Kristallographie und Petrographie der ETHZ, Zürich, for the electron microprobe analysis, and B. Magyar and H. Vetsch, Laboratorium für Festkörperphysik, ETH, Zürich, for the x-ray fluorescence analysis. We also appreciate very much the collaboration with P. E. Lindelof (former P. E. Gregers-Hansen) in the earlier stages of this work.

APPENDIX

In this Appendix we relate the Born expression for the transition probability $w_\sigma^{\sigma'}(\vec{q},\omega)$ to the imaginary part of the (retarded) ion susceptibility function $\chi_{\alpha\beta}(\vec{R},t)$ defined in Eq. (2.3). The ion susceptibility function may be written

$$\chi_{\alpha\beta}(\vec{R},t) = -i \sum_{i,f} e^{(\Omega-E_i)/k_BT}[\langle i|J_\alpha(\vec{R},t)|f\rangle\langle f|J_\beta(\vec{0},0)|i\rangle - \langle i|J_\beta(\vec{0},0)|f\rangle\langle f|J_\alpha(\vec{R},t)|i\rangle]\Theta(t) \quad , \tag{A1}$$

upon introduction of the complete set of ionic states $|f\rangle$. The quantity Ω is the thermodynamic potential entering the thermal average of Eq. (2.3). Upon Fourier transforming with respect to the time and the ionic position $\vec{R}_l$ we get

$$\chi_{\alpha\beta}(\vec{q},\omega) = \sum_l \int dt\, e^{-i(\vec{q}\cdot\vec{R}_l-\omega t)}\chi_{\alpha\beta}(\vec{R}_l,t) = \sum_{i,f} e^{(\Omega-E_i)/k_BT}(1-e^{-(E_f-E_i)/k_BT}) \times \sum_l e^{-i\vec{q}\cdot\vec{R}_l}\frac{\langle i|J_\alpha(\vec{R}_l,0)|f\rangle\langle f|J_\beta(\vec{0},0)|i\rangle}{E_f-E_i+\hbar(\omega+i\eta)} \quad . \tag{A2}$$

Here we have used the usual formula for the time evolution of the operators $J(\vec{R},t)$ and the well-known relation

$$\int_{-\infty}^{\infty} e^{i\omega t}\Theta(t)\,dt = \frac{1}{\omega+i\eta} \quad . \tag{A3}$$

Furthermore we have used that the second term in the sum (A1) is $\exp[(E_i-E_f)/k_BT]$ times the first one as one sees upon interchange of the sum indices i and f.

The Golden Rule expression for $w_\sigma^{\sigma'}(\vec{q},\omega)$ is

$$w_{\sigma}^{\sigma'}(\vec{q},\omega)=\frac{2\pi}{\hbar}\sum_{i,f}e^{(\Omega-E_i)/k_BT}A^2(g-1)^2|\langle\sigma'|\vec{s}|\sigma\rangle\cdot\langle f|\sum_l e^{-i\vec{q}\cdot\vec{R}_l}\vec{J}(\vec{R}_l,0)|i\rangle|^2\delta(E_f-E_i+\hbar\omega)\ , \tag{A4}$$

where $|f\rangle$ and $|i\rangle$ denote final and initial states for the rare-earth ion system, while E_f and E_i are the corresponding energies. When one takes the imaginary part of Eq. (A2) it follows immediately that the expressions (A2) and (A4) may be related as stated in Eq. (2.5).

---

[1]For a general review on singlet-ground-state magnetism see B. R. Cooper, in *Magnetic Properties of Rare Earth Metals,* edited by R. J. Elliott (Plenum, London, 1972), p. 17.

[2]B. R. Cooper and O. Vogt, Phys. Rev. B 1, 1218 (1970).

[3]N. Hessel Andersen, P. E. Gregers-Hansen, E. Holm, H. Smith, and O. Vogt, Phys. Rev. Lett. 32, 1321 (1974).

[4]N. Hessel Andersen, P. E. Lindelof, H. Smith, O. Splittorff, and O. Vogt, Phys. Rev. Lett. 37, 46 (1976).

[5]G. Baym, Phys. Rev. 135, A1691 (1964).

[6]I. Mannari, Prog. Theor. Phys. (Kyoto) 26, 51 (1961).

[7]J. M. Ziman, *Electrons and Phonons,* (Oxford University, New York, 1960).

[8]K. R. Lea, M. J. M. Leask, and W. P. Wolf, J. Phys. Chem. Solids 23, 1381 (1962).

[9]T. M. Holden, E. C. Svensson, W. J. L. Buyers, and O. Vogt, Phys. Rev. B 10, 3864 (1974).

[10]W. Stutius, Phys. Konden. Mater. 9, 341 (1969).

[11]J. W. Cable, J. B. Cowly, B. R. Cooper, J. S. Jacobs, W. C. Koehler, and O. Vogt, in *Proceedings of the 18th Conference on Magnetism and Magnetic Materials, Denver, 1972,* edited by C. D. Graham, Jr. and J. J. Rhyne, AIP Conf. Proc. No. 10 (AIP, New York, 1973), p. 1554.

[12]N. Hessel Andersen, thesis (University of Copenhagen, 1976) (unpublished).

[13]P. M. Levy, J. Phys. C 6, 3545 (1973); C 7, 2760 (1974).

[14]N. Hessel Andersen and O. Vogt, J. Phys. (Paris) 40, C5-118 (1979).

[15]O. Splittorff, thesis (University of Copenhagen, 1976) (unpublished).

[16]P. Fulde and I. Peschel, Adv. Phys. 21, 1 (1972).

[17]T. M. Holden and W. J. L. Buyers, Phys. Rev. B 9, 3797 (1974).

[18]W. J. L. Buyers, T. M. Holden, and A. Perrault, Phys. Rev. B 11, 266 (1975).

[19]H. R. Child, M. K. Wilkinson, J. W. Cable, W. C. Koehler, and E. O. Wollan, Phys. Rev. 131, 922 (1963).

[20]R. Wolseth, *X-ray Energy Spectroscopy* (Kevex Corporation, Burlingame, California, 1973).

[21]J. W. Colby, *Magic IV-A Computer Program for Quantitative Electron Microprobe Analysis* (Bell Telephone Laboratories, Murray Hill, N. J., 1971).

[22]A. E. Stephens, H. J. Malkey, and J. R. Sybert, J. Appl. Phys. 42, 2592 (1971).

[23]K. Carneiro, N. Hessel Andersen, J. K. Kjems, and O. Vogt, in *Proceedings of 2nd International Conference on Crystal Field Effects in Metals and Alloys,* edited by A. Furrer (Plenum, New York, 1977), p. 99.